Available online at www.sciencedirect.com
ScienceDirect
Journal of Sound and Vibration 310 (2008) 512–526
JOURNAL OF SOUND AND VIBRATION
www.elsevier.com/locate/jsvi

The influence of the wake on the stability of cantilevered flexible plates in axial flow

Liaosha Tang*, Michael P. Païdoussis

Department of Mechanical Engineering, McGill University, 817 Sherbrooke St. W., Montreal, Québec, Canada H3A 2K6

Received 30 November 2006; received in revised form 29 August 2007; accepted 20 September 2007
Available online 30 October 2007

Abstract

Cantilevered flexible plates in axial flow lose stability through flutter. Using the inextensibility condition for the cantilevered nonlinear plate equation of motion and the unsteady lumped-vortex model to calculate the fluid loads, a flutter boundary has been obtained. In the time-domain analysis performed to this end, the wake behind the oscillating cantilevered plate is assumed to issue tangentially from the free trailing edge and extend downstream with an undulating form. The influence of the wake on system stability may be characterized in terms of the non-dimensional mass ratio, reduced flow velocity and flutter frequency. For large values of the mass ratio, the plate vibrates with high frequency and high-order mode content. It is shown that the wake has less influence on system stability for long plates than it does for short ones.

1. Introduction

Cantilevered flexible plates in axial flow lose stability through flutter. A schematic diagram of this fluid–structure interaction system is shown in Fig. 1. The physical parameters for the rectangular homogeneous plate are its length L, thickness h ($h \ll L$), material density ρ_P and bending stiffness $D = Eh^3/[12(1-\nu^2)]$, where E and ν are, respectively, Young's modulus and the Poisson ratio of the plate material. The plate is clamped at its upstream edge; all other edges are free. An upstream rigid segment of length L_0 is considered for the clamping constraint. The spanwise dimension of the plate is supposed to be infinite. Therefore, both the plate and the corresponding fluid flow surrounding the plate are considered to be two-dimensional. The fluid flow, of density ρ_F, passes over both surfaces of the plate from the clamped upstream edge to the free trailing edge with mean undisturbed flow velocity U. The plate remains in a static flat state when U is low; any small disturbance introduced to the system is attenuated. However, when U is sufficiently high and exceeds a critical value U_c, flutter takes place.

The stability of cantilevered flexible plates in axial flow was first studied by Taneda [1] in 1968. From then on, extensive research has been conducted on this problem [2–20]; detailed literature reviews may be found in

*Corresponding author.
E-mail address: liaosha.tang@mail.mcgill.ca (L. Tang).

0022-460X/$ - see front matter © 2007 Elsevier Ltd. All rights reserved.
doi:10.1016/j.jsv.2007.09.025

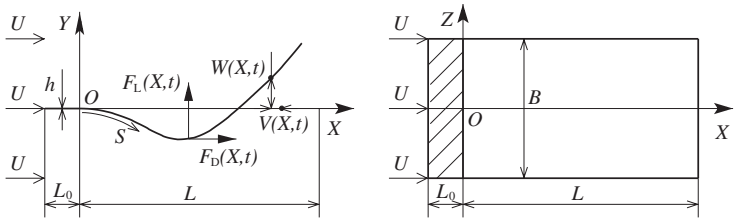

Fig. 1. A cantilevered flexible plate in axial flow.

Refs. [21, Chapter 10; 22]. The current paper is a continuation of the work conducted by Tang and Païdoussis [22]; a nonlinear equation of motion has been utilized, assuming the middle plane of the plate to be inextensible, together with the unsteady lumped-vortex model [23] for calculating the unsteady fluid loads. This theoretical model is used to predict the flutter boundary. The flutter boundary thus obtained is compared with all available experimental data and previous theoretical predictions. It is found that, when the plate is long, the various available theories are in very good agreement with each other as well as with measurements from different experiments. In contrast, agreement between the various theories and with experiments is rather poor for short plates. The present paper aims to correlate these observations to the influence of the wake beyond the trailing edge of the plate. It is proposed that the wake has much less influence on the stability of the fluid–structure interaction system for long plates than it does for short ones.

2. The numerical model

As it has been discussed in detail in the precursor paper [22] to the present one, only a brief account of the numerical model is presented here. Based on the inextensibility condition and following Semler et al. [24], the partial differential equation governing plate motion is found to be

$$\begin{aligned}&\rho_P h\ddot{W} + D\left(1 + a\frac{\partial}{\partial t}\right)[W''''(1 + W'^2) + 4W'W''W'''' + W''^3]\\&\quad + \rho_P h W' \int_0^S (\dot{W}'^2 + W'\ddot{W}')\,\mathrm{d}S - \rho_P h W'' \int_S^L \int_0^S (\dot{W}'^2 + W'\ddot{W}')\,\mathrm{d}S\,\mathrm{d}S\\&\quad = F_L - W'F_D + W'' \int_S^L F_D\,\mathrm{d}S,\end{aligned} \tag{1}$$

$$V = -\frac{1}{2}\int_0^S W'^2\,\mathrm{d}S, \tag{2}$$

where, as shown in Fig. 1, W and V are, respectively, the transverse and longitudinal displacements of the plate; S is the distance of a material point on the plate from the origin, measured along the plate centreline in a coordinate system embedded in the plate; F_L and F_D are, respectively, the transverse and longitudinal fluid loads acting on the plate; a is the material damping coefficient, assuming a Kelvin–Voigt model [25]. The overdot and the prime, respectively, represent temporal and spatial derivatives, i.e., $\partial(\,)/\partial t$ and $\partial(\,)/\partial S$.

If one is concerned with the flutter boundary only, the plate transverse displacement W can be assumed to be very small, i.e., $W \ll L$, and the plate longitudinal displacement V can consequently be neglected. Moreover, in this case, the measured S can be regarded as being identical to the coordinate X in the fixed X–Y system. Using the plate length L as the length scale, the characteristic time of free vibration of the plate *in vacuo*, $\sqrt{\rho_P h L^4/D}$, as the time scale, and the dynamic pressure, $\rho_F U^2$, as the scale for normalizing fluid loads, Eq. (1)

may be written in the non-dimensional form

$$\ddot{w} + \left(1 + \alpha\frac{\partial}{\partial\tau}\right)[w''''(1+w'^2) + 4w'w''w''' + w''^3] + w'\int_0^x (\dot{w}'^2 + w'\ddot{w}')\,\mathrm{d}x - w''\int_x^1\left[\int_0^x (\dot{w}'^2 + w'\ddot{w}')\,\mathrm{d}x\right]\mathrm{d}x = \mu U_R^2\left(f_L - w'f_D + w''\int_x^1 f_D\,\mathrm{d}x\right), \tag{3}$$

where the overdot and the prime, from now on, represent $\partial(\,)/\partial\tau$ and $\partial(\,)/\partial x$, respectively; $\alpha = a/\sqrt{\rho_P h L^4/D}$ is the non-dimensional material damping coefficient. The two main non-dimensional system parameters are the mass ratio μ and reduced flow velocity U_R, arising from the fluid–structure interaction; they are defined by

$$U_R = UL\sqrt{\frac{\rho_P h}{D}} \tag{4}$$

and

$$\mu = \frac{\rho_F L}{\rho_P h}. \tag{5}$$

As illustrated in Fig. 2, a panel method, in particular the unsteady lumped-vortex model, is used to calculate the fluid loads acting the plate; a detailed discussion on the implementation of this scheme may be found in Ref. [22]. Generally speaking, at a given time step $k+1$, the bound vortices Γ_i^{k+1} $(i = 1, 2, \ldots, N)$ and the latest wake vortex Γ_{N+1}^{k+1} (i.e., $\Gamma_{W_1}^{k+1}$) can be obtained using the panel method, where N is the number of panels. The fresh wake vortex $\Gamma_{W_1}^{k+1}$ is supposed to be born at a location along the tangential prolongation of the last panel and have a longitudinal clearance of $0.25U\Delta t$ to the trailing edge of the plate; the strength of $\Gamma_{W_1}^{k+1}$ is determined according to Kelvin's circulation theorem [26]. Once a wake vortex is in place, it is supposed to move downstream with the undisturbed flow velocity U for simplicity; the influence on its motion of the bound vortices and the other wake vortices is neglected. Moreover, no wake dissipation or vortex–vortex interaction are considered. Therefore, as shown in Fig. 2, an undulating vortex street is formed, and the longitudinal distance between two successive wake vortices, for example Γ_{N+1}^{k} and Γ_{N+1}^{k-1}, is always $U\Delta t$. When the bound vortices and the latest wake vortex are available at the current time step, together with previously generated wake vortices, the pressure difference ΔP across the plate can be calculated. ΔP is subsequently decomposed into the lift F_L and the drag F_D, which are inserted into the right-hand side of Eq. (1). As illustrated in Fig. 2, in addition to the inviscid drag obtained from the decomposition of ΔP, a viscous component of drag $\rho_F U^2 C_D$ may be incorporated in F_D, where C_D is the viscous drag coefficient. In the fluid-dynamic calculations,

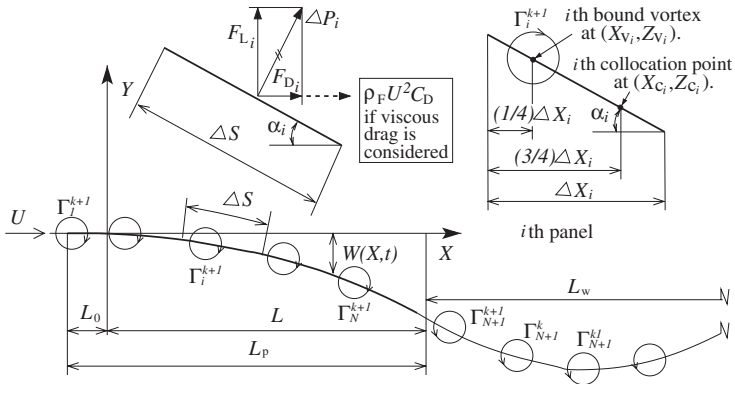

Fig. 2. The panel method applied to a cantilevered flexible plate in axial flow.

all spatial variables are normalized by L and the flow velocity by U; for example, the dimensional truncated wake length L_W and vortex strength Γ and their corresponding non-dimensional counterparts l_W and γ are related by $l_W = L_W/L$ and $\gamma = \Gamma/(UL)$.

The traditional Galerkin method is applied to Eq. (3) by assuming that the plate transverse deformation can be expanded in terms of generalized coordinates $q_m(\tau)$ and the linear *in vacuo* cantilevered beam eigenfunctions $\phi_m(x)$ [27] as

$$w(x,\tau) = \sum_{m=1}^{M} q_m(\tau)\phi_m(x), \tag{6}$$

where M is the number of modes utilized in the analysis, leading to the following equation:

$$\begin{aligned} f_i = {} & \ddot{q}_i + A_i q_i + \alpha A_i \dot{q}_i + B_{imnl} q_m q_n q_l + \alpha B_{imnl}(\dot{q}_m q_n q_l + q_m \dot{q}_n q_l + q_m q_n \dot{q}_l) \\ & + C_{imnl} q_m (\dot{q}_n \dot{q}_l + q_n \ddot{q}_l), \end{aligned} \tag{7}$$

where Einstein's scientific notation has been used, and the range of all indices i, l, m and n is from 1 to M. The generalized load f_i is given by

$$f_i = \mu U_R^2 \int_0^1 \left(f_L - w' f_D + w'' \int_x^1 f_D \, \mathrm{d}x \right) \phi_i \, \mathrm{d}x. \tag{8}$$

Finally, the constant coefficients A_i, B_{imnl} and C_{imnl} are:

$$A_i = \beta_i^4, \tag{9}$$

$$B_{imnl} = \int_0^1 \phi_i (\phi_m'''' \phi_n' \phi_l' + 4\phi_m' \phi_n'' \phi_l''' + \phi_m'' \phi_n'' \phi_l'') \, \mathrm{d}x, \tag{10}$$

$$C_{imnl} = \int_0^1 \phi_i' \phi_m' \left[\int_x^1 \left(\int_0^\eta \phi_n' \phi_l' \, \mathrm{d}\zeta \right) \mathrm{d}\eta \right] \mathrm{d}x, \tag{11}$$

where β_i is the ith dimensionless eigenvalue of a cantilevered beam [27].

Eq. (7) can be solved using a suitable time integration scheme [22], e.g. the fourth-order Houbolt method.

3. The flutter boundary

The flutter boundary predicted by the present theory is shown in Fig. 3, where the mass ratio is rewritten in the form $\mu = [\rho_F/(\rho_P h)]L$, and the ordinate U_{R_c}/μ can be interpreted as $U_{R_c}/\mu = [(\rho_P h)^{3/2}/(\rho_F D^{1/2})]U_c$. Therefore, when the physical parameters ρ_P, h, D and ρ_F of the fluid–structure interaction system are fixed, the U_{R_c}/μ versus μ plot actually represents the dependence of the dimensional critical flow velocity U_c on the plate length L.

In Fig. 3, the flutter boundaries predicted by Huang [8], Guo and Païdoussis [10], Yamaguchi et al. [11], Watanabe et al. [14], Argentina and Mahadevan [17], Shelley et al. [18] and Eloy et al. [20] and the experimental data published by Kornecki et al. [6], Huang [8], Yamaguchi et al. [12], Watanabe et al. [13], Tang et al. [15] and Souilliez et al. [19] are also presented. All flutter boundaries in Fig. 3 obtained by various theories and from experiments exhibit a clear overall trend: U_c decreases with increasing L (excepting a local rise and subsequent subsidence for the flutter boundary predicted by the present theory within the range $1.0 < \mu < 1.2$, caused by a subtle mode transition [22]).

It can be observed in Fig. 3 that U_c is very sensitive to L when the plate is short (i.e., $\mu < 1$); while, for long plates (i.e., $\mu > 4$), U_c varies very gradually with changing L. Another important observation that can be made in Fig. 3 is that the differences in the flutter boundaries obtained using various theories are quite large for short plates ($\mu < 1$). Gradually and monotonically, this difference is diminished as L is increased, and all theories converge towards one another for long plates ($\mu > 4$). The same phenomenon can also be observed regarding the agreement between experimental data (excepting those by Watanabe et al. [13]) and theoretical predictions.

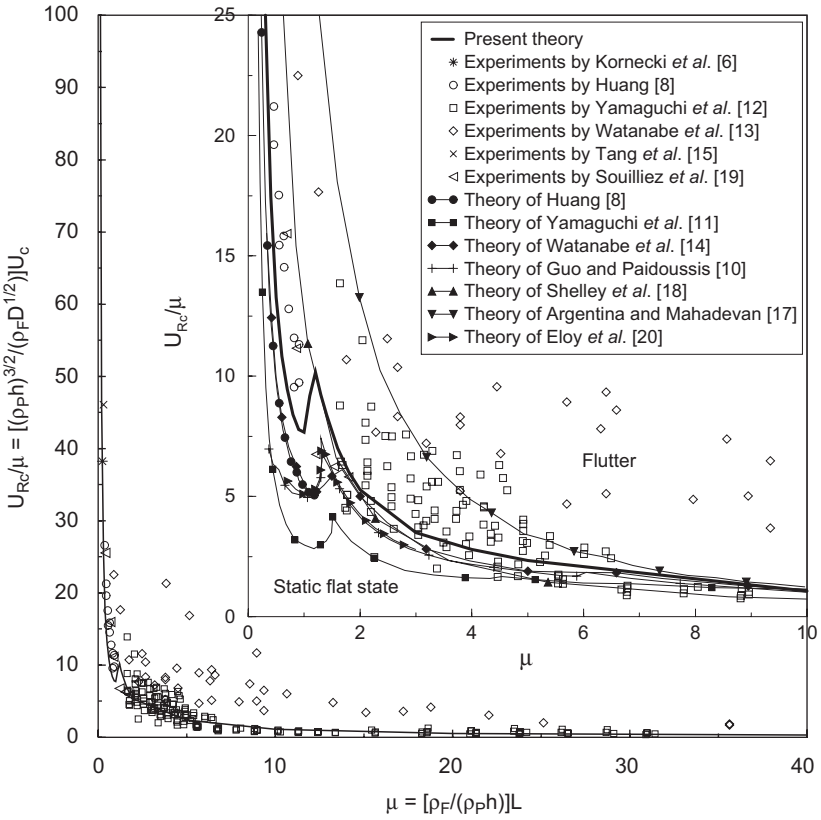

Fig. 3. The flutter boundary of cantilevered flexible plates in axial flow: theoretical predictions and experimental measurements from various sources. For the present theory, the results shown were obtained with the system parameters: $l_0 = 0.01$, $\alpha = 0.004$ and $C_D = 0$.

Table 1
The values of $\rho_F/(\rho_P h)$ and $(\rho_P h)^{3/2}/(\rho_F D^{1/2})$ in various experiments

Experiments by	$\rho_P h$ (kg/m^2)	ρ_F (kg/m^3)	D (N m)	$\frac{\rho_F}{\rho_P h}$ (m^{-1})	$\frac{(\rho_P h)^{3/2}}{\rho_F D^{1/2}}$ (s/m)
Kornecki et al. [6]	1.343	1.226	8.47×10^{-1}	0.913	1.397
Huang [8]	0.142	1.226	7.29×10^{-4}	8.634	1.616
Tang et al. [15]	1.108	1.226	3.83×10^{-1}	1.107	1.50
Souilliez et al. [19]	0.2	1.226	6.15×10^{-3}	6.31	0.93

It should be emphasized that Fig. 3 reveals inherent properties of the global stability of cantilevered flexible plates in axial flow. Both the trend of a single flutter boundary and the relation between different ones (no matter whether they be theoretical or experimental) are neither distorted by scale factors in the axes used nor qualitatively changed by other factors influencing the system dynamics (i.e., the length of upstream rigid segment $l_0 = L_0/L$, the material damping coefficient α, and the viscous drag coefficient C_D). The actual values of the scale factors $[\rho_F/(\rho_P h)]$ and $[(\rho_P h)^{3/2}/(\rho_F D^{1/2})]$ for some of the experimental data [6,8,15,19] are listed in Table 1; the absence of the others [12,13] from this table is due to the lack of published information which would have enabled calculation of these scale factors. Although the scale factors for L and U_c may not always be close to unity nor be the same for individual experiments, it is easy to check that they will not *qualitatively* change the key properties of the flutter boundaries shown in Fig. 3. Moreover, although the system dynamics

is also dependent on the values of the other parameters, i.e., l_0, α and C_D, the choice of values for these parameters will not cause a qualitative change to the flutter boundary [22].

It should be mentioned that Lemaitre et al. [5] also have recently reported that U_c is insensitive to L for long plates, in their work on hanging plates in axial flow (i.e., with gravity in the positive X direction of Fig. 1); they attributed the observed trend to the axial tension caused by the distributed weight of the plate. However, for all the theoretical analyses and experiments presented in Fig. 3, both the plate and the upstream support are vertical (i.e., gravity is in the negative Z direction of Fig. 1), and hence gravity needs not be taken into account.

If, instead of U_{R_c}/μ one had plotted U_{R_c} versus μ (refer to Fig. 7 of Ref. [22]), neither the global trend for a single flutter boundary nor the correlation between different ones as described in the foregoing would be discernible. Therefore, a discussion of the global properties of a flutter boundary has to be conducted in terms of dimensional parameters U_c and L in a U_{R_c}/μ versus μ plot. The scale factor $[\rho_F/(\rho_P h)]$ for different systems is not always the same, and a system with a larger μ does not necessarily correspond to a longer plate than another system with a smaller μ. However, for a specific system of which the parameters ρ_P, h and ρ_F are fixed, μ is directly proportional to L. In particular, in light of the flutter boundary predicted by the present theory, one can consider that a plate is long when $\mu \geqslant 4$, and that it is a short one when $\mu \leqslant 1$.

4. Oscillation characteristics on the flutter boundary

The characteristics of the system along the flutter boundary are studied first. Four points, at $\mu = 0.2$ and 0.6 for short plates and $\mu = 4$ and 20 for long ones, are selected, and the computed time history, frequency and vibration mode at the critical point U_{R_c} for each μ are obtained using the present theory; they are shown in Figs. 4 and 5.

It should be mentioned that the parameters involved in these simulations, including U_R, initial conditions, time step $\Delta\tau$ and stop-time τ_E (listed in Table 2) are not the same for all values of μ. First, as U_{R_c} varies with μ, the value of U_{R_c} in each case is different. One may notice in Table 2 that the relation between U_{R_c} and μ exhibits an irregular pattern (see also Fig. 7 in Ref. [22]). In particular, $U_{R_c} = 9.92$, 6.71, 10.15 and 8.71, respectively, for $\mu = 0.2$, 0.6, 4 and 20. As mentioned in Section 3, this is not a global trend such as that observed in the U_{R_c}/μ versus μ plot of Fig. 3. Secondly, the time step $\Delta\tau$ in each simulation is determined by the requirement of convergence; it is not necessarily the same for different μ. Note the number of discrete point vortices N_W in a fixed length of truncated wake l_W is related to $\Delta\tau$ by

$$N_W = \frac{L_W}{U\Delta t} = \frac{l_W}{U_R\Delta\tau}, \tag{12}$$

where Δt is the dimensional time step and l_W is the non-dimensional truncated wake length; $l_W = 9$ is used in the present study. Finally, as seen in Table 2, different initial conditions and stop times τ_E are used for different cases of μ (the common part of the initial conditions, not listed in Table 2, is $q^0_{i,i\neq 1} = 0$, $\dot{q}^0_i = 0$). The purpose here is to obtain comparable flutter amplitudes $\max(|w(x = 1)|)$ for all the values of μ tested, at a time instant close to τ_E, and consequently to ensure that the corresponding wakes have roughly the same strength. Since each simulation is carried out with the corresponding U_{R_c}, the time histories (still transient, not quite steady state) in Fig. 4 have a very small growth rate. Values of $\max(|w(x = 1)|)$ at a time instant close to τ_E are listed in Table 2; it can be seen that they are approximately the same.

It can be seen in Fig. 4 that the non-dimensional frequency $f^\star = f\sqrt{\rho_P h L^4/D}$ increases with μ. In particular, as listed in Table 2, $f^\star_c = 2.8$, 2.8, 5.2 and 5.8, respectively, for $\mu = 0.2$, 0.6, 4 and 20.

The instantaneous shapes of the oscillating plates at a series of successive time steps for $\mu = 0.6$, 4 and 20 are shown in Fig. 5; each series roughly constitutes a half cycle of the oscillation. It can be seen in Figs. 5(a–c) that the plate basically oscillates in a second beam-mode for $\mu = 0.6$ (and also for $\mu = 0.2$, not shown); the third beam-mode and higher modes contribute a negligible part to the vibration. However, the third beam-mode component becomes comparable to that of the second beam-mode when $\mu = 4$, and it becomes the dominant one for $\mu = 20$. The local extrema along the oscillating plate are marked with small circles in Fig. 5; it can be seen that a wave travels downstream for all cases of μ. Although it is clear in Fig. 5 that the wave travels with a higher speed for long plates (for $\mu = 4$ and 20) than it does for the short one ($\mu = 0.6$), the phase velocity is not significantly different for $\mu = 4$ and 20.

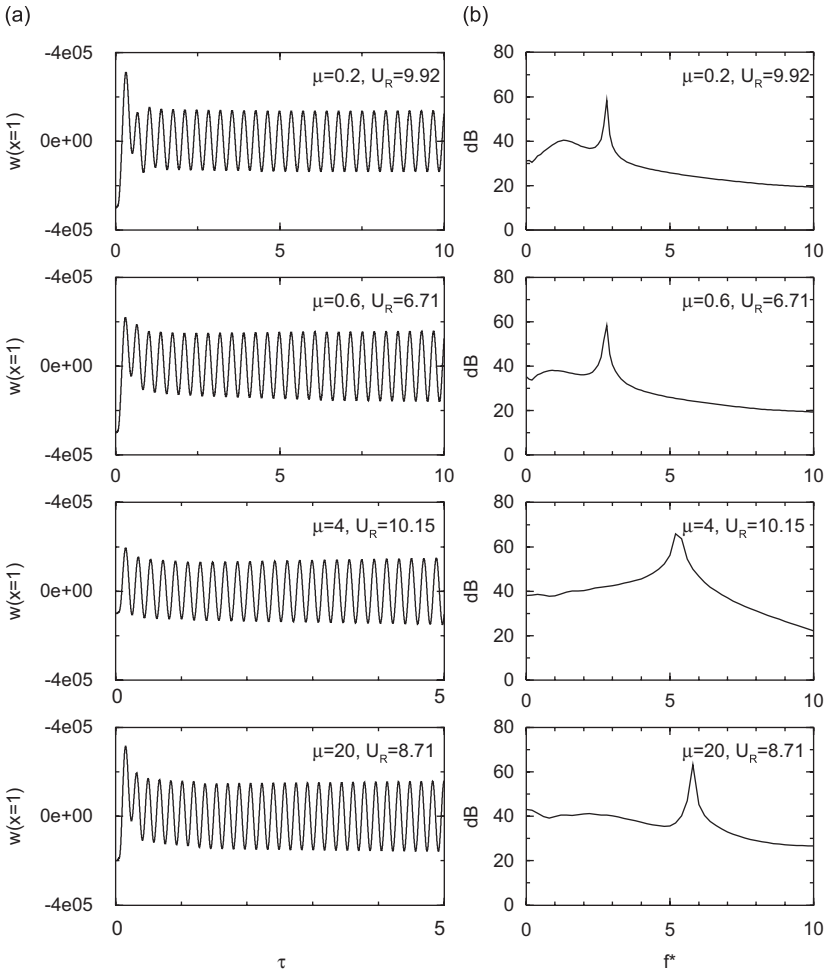

Fig. 4. (a) The time histories and (b) PSDs showing flutter frequencies, for the chosen values of mass ratio μ. The other system parameters are: $l_0 = 0.01$, $\alpha = 0.004$ and $C_D = 0$.

5. The influence of the wake

Why do theoretical predictions and experimental measurements generally display better agreement for long plates than they do for short ones? Although, of course, a wake always exists in all experiments, there are important differences among various theories as to the treatment accorded to the wake behind the plate. In particular, Huang [8], Watanabe et al. [13] and Argentina and Mahadevan [17] used Theodorsen's theory [28] or one of its modified versions, and considered a wake behind the plate along the neutral plane ($Y = 0$, see Fig. 1). Yamaguchi et al. [11] adopted the linearly-varying vortex sheet model [23] and Tang et al. [15] used a vortex lattice model for calculating fluid loads; both included a wake behind the plate along the neutral plane. Guo and Païdoussis [10] and Eloy et al. [20] tried direct solutions of the potential flow problem for the fluid part of the system and completely neglected the wake. Shelley et al. [18] applied localized excitation theory [29] without taking the wake into account. Finally, the present theory works with the lumped-vortex model and considers a wavy wake street. An important conclusion can be reached from this compact literature review: that the wake must have but a small influence on system stability when the plate is sufficiently long.

In Fig. 6, for $\mu = 0.2$, 0.6, 4 and 20, the strength of the discrete point vortices γ_W in the wake is plotted against their longitudinal coordinate x_W. The time instants for these plots are selected using the same rule as that for determining $\tau^\star$ in Fig. 5: i.e., a time instant close to τ_E is chosen, such that at that moment the plate tip

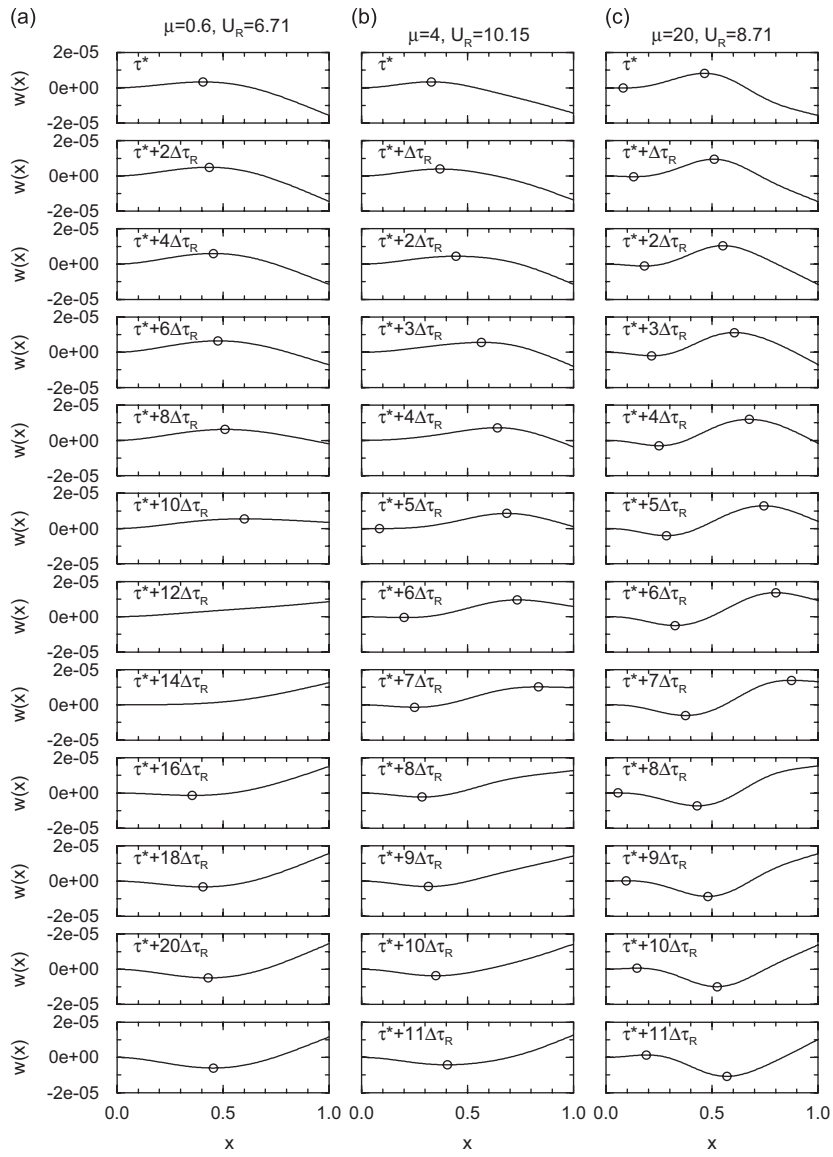

Fig. 5. The flutter modes of the system for the chosen values of mass ratio μ: (a) $\mu = 0.6$, (b) $\mu = 4$ and (c) $\mu = 20$. Here $\tau^\star$ is a selected time instant close to τ_E, such that at this moment the plate tip reaches its maximum negative displacement, which is not necessarily the same for all values of μ; $\Delta\tau_R = 0.001$ is the non-dimensional time step for recording the plate shapes. The other system parameters used are: $l_0 = 0.01$, $\alpha = 0.004$ and $C_D = 0$.

reaches its maximum negative displacement. It can be seen in Fig. 6 that the γ_W versus x_W plot also has a wavy form. Note that both the x_W–γ_W and the x_W–y_W waves (as illustrated in Fig. 2) have the same wavelength and phase. In the current study of the flutter boundary, the vibration amplitude of the plate is always very small (of the order of 10^{-5}, see Figs. 4 and 5), i.e., $\max(|y_W|) = \max(|w(x = 1)|) \ll 1$. Therefore, all wake vortices may be regarded as lying along the neutral plane ($y = 0$) when one considers the influence of the wake on the plate.

Two factors affecting the influence of the wake on the plate are its vortical strength and distribution in space. The strength for a wake consisting of discrete point vortices (as obtained using the present theory) should be determined by the number of wake vortices N_W in a fixed truncated wake length l_W ($l_W = 9$ in the present study) and the strength of each individual vortex γ_W. Without considering the distribution and the

Table 2
Simulation conditions and results for various values of μ

μ	Short plates		Long plates	
	0.2	0.6	4	20
Simulation conditions				
U_{R_c}	9.92	6.71	10.15	8.71
Initial condition q_1^0 ($\times 10^{-5}$)	-1.5	-1.5	-5.0	-1.0
$\Delta\tau$	0.001	0.001	0.0001	0.0001
τ_E	10	10	5	5
Simulation results				
$\max(\lvert w(x=1)\rvert)$ ($\times 10^{-5}$)	1.4	1.6	1.5	1.6
$f^\star$	2.8	2.8	5.2	5.8
Dominant mode	2nd	2nd	2nd and 3rd	3rd

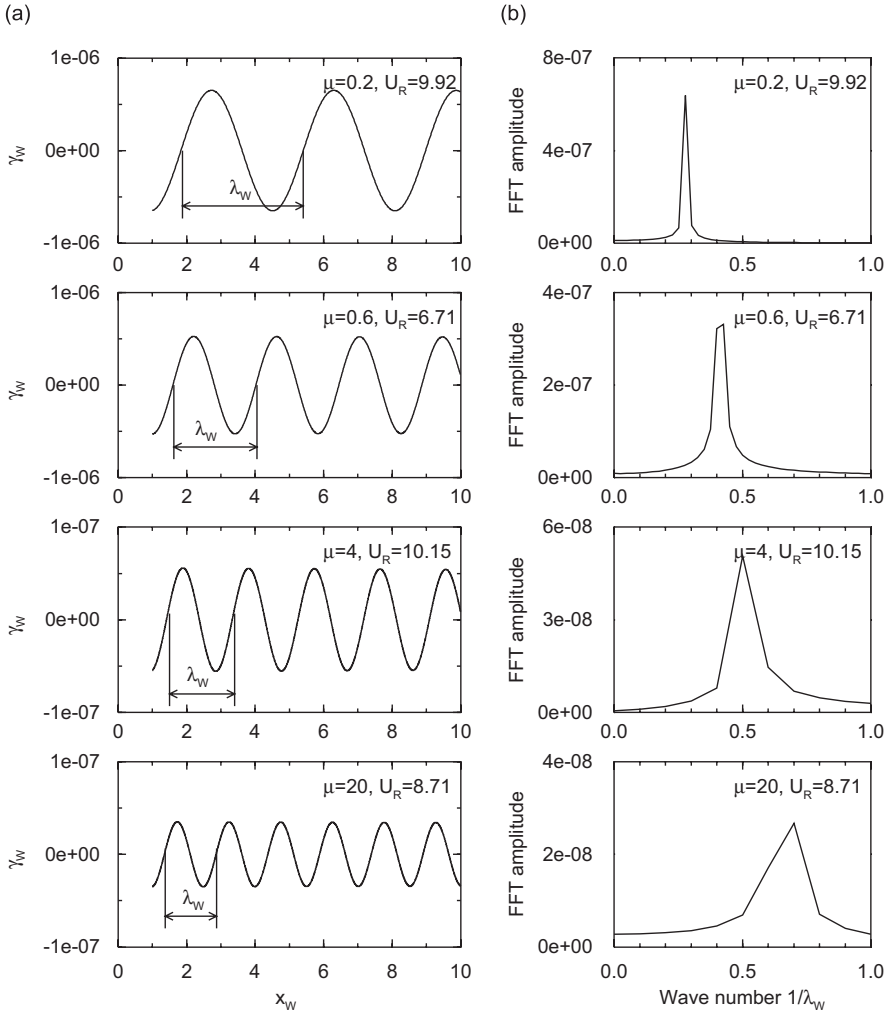

Fig. 6. The instantaneous wake for the chosen values of mass ratio μ: (a) the distribution of the wake vortices in space; (b) the FFT amplitude as a function of the wavenumber $1/\lambda$. For each μ, the wake street was obtained using the corresponding U_{R_c}. The other system parameters are: $l_0 = 0.01$, $\alpha = 0.004$ and $C_D = 0$.

Table 3
Equivalent strength of wake vorticity and wake-induced flow velocity at $x_0 = 0.5$

μ	Short plates		Long plates	
	0.2	0.6	4	20
N_W ($l_W = 9$)	907	1341	8867	10333
$1/\lambda_W$	0.28	0.42	0.5	0.7
$\max(\lvert\gamma_W\rvert) \times 10^7$	6.51	5.26	0.559	0.351
$N_W \times \max(\lvert\gamma_W\rvert) \times 10^4$	5.90 (100%)	7.05 (119%)	4.96 (84%)	3.63 (62%)
$w_W(x_0 = 0.5) \times 10^5$	3.22 (100%)	2.97 (92.9%)	0.65 (20%)	0.53 (16%)

strength variation of wake vortices in space, one may use $N_W \times \max(|\gamma_W|)$ as a rough indicator of the equivalent strength for a wake having a regular wavy form. The equivalent strengths $N_W \times \max(|\gamma_W|)$ calculated for individual cases of μ are listed in Table 3.

Also, the wake-induced flow velocity (the *downwash*) w_W at a point $(x = x_0, y = 0)$ on the plate can be calculated by

$$w_W(x_0) = \frac{1}{2\pi}\sum_{j=1}^{N_W}\frac{\gamma_{W_j}}{x_{W_j} - x_0}, \tag{13}$$

where the distribution of wake vortices in space has been taken into account. The calculated $w_W(x_0 = 0.5)$, also listed in Table 3, can be regarded as an evaluation of the influence of the wake on the plate when comparing various cases of μ.

In Table 3, the calculated values of $N_W \times \max(|\gamma_W|)$ and $w_W(x_0 = 0.5)$ are expressed as a percentage of those for the reference case of $\mu = 0.2$. It can be seen that the equivalent strengths of the wake, $N_W \times \max(|\gamma_W|)$, for the various cases of μ are similar. In contrast, the wake-induced flow velocity, $w_W(x_0 = 0.5)$, decreases significantly as μ increases. It is easy to prove that the decrease of w_W with increasing μ is due to the variation of wavelength of the wake λ_W as shown in Fig. 6 and also listed in Table 3 in terms of the wavenumber $1/\lambda_W$. For a shorter wavelength λ_W (i.e., a larger wavenumber $1/\lambda_W$), successive effective wake vortices with alternating positive and negative signs (refer Fig. 2 in Ref. [3]) come closer to each other; and thus the wake has a smaller overall influence (in terms of w_W) on the plate. Note that λ_W is related to $f^\star$ through

$$\lambda_W = \frac{U_R}{f^\star}. \tag{14}$$

Therefore, as μ increases, the decrease in λ_W is actually caused by the increase in the flutter frequency $f^\star$ of the plate.

When evaluating the influence of the wake on the plate, one has to consider the plate motion as well. In Fig. 7, the plate displacement $w(x)$ along the plate, the vibration velocity $\mathrm{d}w(x)/\mathrm{d}\tau$, the wake-induced flow velocity $w_W(x)$, as well as the ratio $(\mathrm{d}w(x)/\mathrm{d}\tau)/(w_W(x)U_R)$ are presented for $\mu = 0.2$, 0.6, 4 and 20. Note that the presence of U_R in the ratio arises from non-dimensionalization, i.e.,

$$\frac{\mathrm{d}W(X)/\mathrm{d}t}{W_W(X)} = \frac{L\,\mathrm{d}w(x)/(\sqrt{\rho_P h L^4/D}\,\mathrm{d}\tau)}{U w_W(x)} = \frac{1}{UL}\sqrt{\frac{D}{\rho_P h}}\frac{\mathrm{d}w(x)/\mathrm{d}\tau}{w_W(x)} = \frac{\mathrm{d}w(x)/\mathrm{d}\tau}{w_W(x)U_R}, \tag{15}$$

where $W_W(X)$ is the dimensional wake-induced flow velocity. For each μ, the time instant for the data presented is again selected from a point close to τ_E, and at this moment the plate tip should reach its negative maximum displacement, as shown in Fig. 7(a).

It can be seen in Fig. 7(b) that the $w_W(x)$ versus x curves are qualitatively similar, and at a fixed point on the plate the magnitude of $w_W(x)$ decreases monotonically as μ is increased due to the increase in flutter frequency $f^\star$.

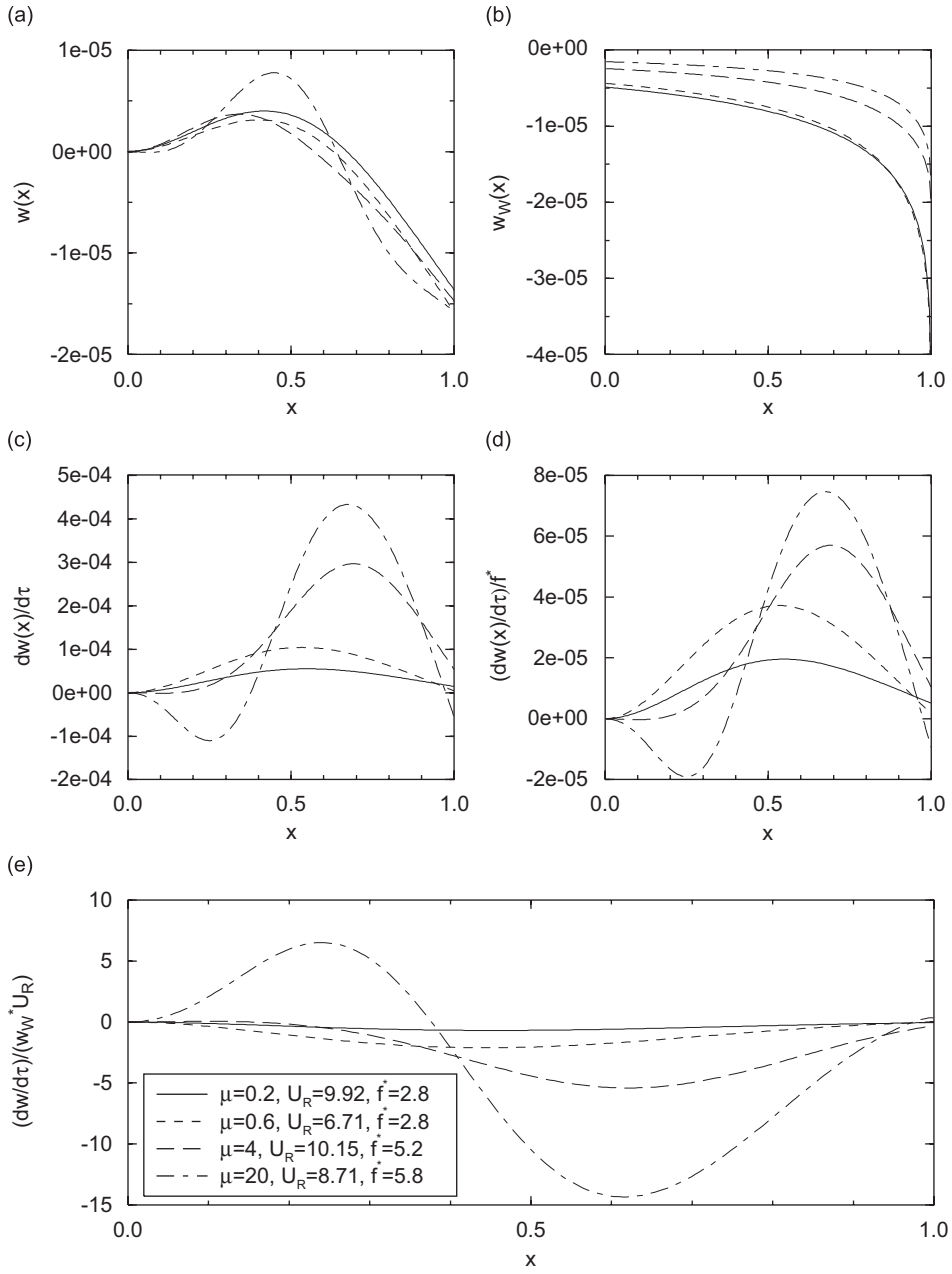

Fig. 7. The evaluation of the influence of the wake for the chosen values of mass ratio μ: (a) the flutter modes; (b) the wake-induced flow velocities; (c) the vibration velocities of the plates; (d) the normalized vibration velocities of the plates; and (e) the ratios of the vibration velocities of the plates to the wake-induced flow velocities. The other system parameters are: $l_0 = 0.01$, $\alpha = 0.004$ and $C_D = 0$.

The plate vibration velocity $\mathrm{d}w(x)/\mathrm{d}\tau$, for all values of μ under consideration, is plotted in Fig. 7(c). Note that $\mathrm{d}w(x)/\mathrm{d}\tau$ is the instantaneous velocity distribution along the plate, which is a function not only of the flutter frequency $f^\star$ but also of the vibration mode. In order to examine the influence of the vibration mode, the normalized plate vibration velocities, defined by $(\mathrm{d}w(x)/\mathrm{d}\tau)/f^\star$, are plotted in Fig. 7(d). It can be seen that, because higher-order modes present in the flutter become more important for the systems with larger μ, the overall magnitude of $(\mathrm{d}w(x)/\mathrm{d}\tau)/f^\star$ increases with increasing μ, although the instantaneous plate shapes $w(x)$ for all cases of μ are roughly the same (see Fig. 7(a)).

Finally, in Fig. 7(e), the plots of $(\mathrm{d}w(x)/\mathrm{d}\tau)/(w_W U_R)$ are used for a comparison of the influence of the wake on the plate for the cases of μ under consideration. It can be observed that, with increasing μ, the overall magnitude of $(\mathrm{d}w(x)/\mathrm{d}\tau)/(w_W U_R)$ grows significantly.

In summary, quantitative evaluations of the wake-induced flow velocity $w_W(x)$, the plate vibration velocity $\mathrm{d}w(x)/\mathrm{d}\tau$ and the ratio $(\mathrm{d}w(x)/\mathrm{d}\tau)/(w_W(x)U_R)$, for individual cases of μ, in terms of the area enclosed by the curves shown in Figs. 7(b), (c) and (e) and the x-axis are listed in Table 4. It can be seen that $\int_0^1 |(\mathrm{d}w(x)/\mathrm{d}\tau)/(w_W(x)U_R)|\,\mathrm{d}x = 0.386$, 1.13, 2.41 and 6.31 for $\mu = 0.2$, 0.6, 4 and 20, respectively. That is, w_W becomes increasingly less important than $\mathrm{d}w(x)/\mathrm{d}\tau$ as μ is increased. Note that this trend is caused not only by the decrease in $\int_0^1 |w_W(x)|\,\mathrm{d}x$ but also by the increase in $\int_0^1 |\mathrm{d}w(x)/\mathrm{d}\tau|\,\mathrm{d}x$ as μ is increased; i.e., the wake-induced velocity on the plate, w_W, is diminished, as compared to the transverse velocity of the plate.

Furthermore, although it does not reveal the underlying mechanism, the most direct way for assessing the influence of the wake on system stability is to find a new critical point $U^{\star}_{R_c}$ with a modified model *excluding* the wake and to compare it with U_{R_c} obtained with the full model. For each case of μ, the critical values U_{R_c} and $U^{\star}_{R_c}$ are listed in Table 5. When μ grows from 0.2 to 0.6 and then to 4, it can be seen that the difference between U_{R_c} and $U^{\star}_{R_c}$ decreases. For $\mu = 20$, however, $|U_{R_c} - U^{\star}_{R_c}| = 0.5$, which does not follow this decreasing trend. Nevertheless, when the value of $|(U_{R_c}/\mu) - (U^{\star}_{R_c}/\mu)|$ is evaluated, a sharp decreasing trend with respect to μ can be observed for all values of μ under consideration. Therefore, for fixed physical parameters ρ_P, h, D and ρ_F of the system, one can draw the conclusion that the wake has a diminishing influence on system stability as the length of the plate is increased. That is, the *dimensional* critical flow velocity U_c for long plates is little affected by the wake, whereas this is not true for short plates.

Regarding the large values of $|(U_{R_c}/\mu) - (U^{\star}_{R_c}/\mu)|$ for $\mu = 0.2$ and 0.6, as listed in Table 5, one can also conclude that the wake has an important influence on system stability for short plates, the underlying mechanism of which may be illustrated using the diagram in Fig. 8. Note that, for a case of small μ, the plate vibrates in the second beam-mode (see the curve $w(x)$ for $\mu = 0.2$ in Fig. 7(a)), and one can approximately consider the flexible plate, at a given time instant, as a rigid thin cambered airfoil moving upward with a velocity $\mathrm{d}W/\mathrm{d}t$, as shown in Fig. 8, and also be subjected to a wake-induced velocity W_W. The directions of $\mathrm{d}W/\mathrm{d}t$ and W_W are determined, respectively, in accordance with the signs of $\mathrm{d}w(x)/\mathrm{d}\tau$ and $w_W(x)$ shown in Fig. 7 for $\mu = 0.2$. It can be seen in Fig. 8 that, when W_W is equal to or larger than $\mathrm{d}W/\mathrm{d}t$ (refer to the value of $\int_0^1 |(\mathrm{d}w(x)/\mathrm{d}\tau)/(w_W(x)U_R)|\,\mathrm{d}x$ listed in Table 4 for $\mu = 0.2$), the neglect of W_W will decrease the angle θ and

Table 4
An evaluation of influence of the wake on system stability and the underlying mechanism

μ	Short plates		Long plates	
	0.2	0.6	4	20
$\int_0^1 \lvert w_W(x)\rvert\,\mathrm{d}x \times 10^6$	9.97 (100%)	9.60 (96%)	5.30 (53%)	3.62 (36%)
$\int_0^1 \left\lvert \frac{\mathrm{d}w(x)}{\mathrm{d}\tau} \right\rvert \mathrm{d}x \times 10^5$	3.37 (100%)	5.98 (177%)	13.5 (399%)	18.4 (545%)
$\int_0^1 \left\lvert \frac{\mathrm{d}w(x)/\mathrm{d}\tau}{w_W(x)U_R} \right\rvert \mathrm{d}x$	0.39 (100%)	1.13 (292%)	2.41 (624%)	6.31 (1637%)

Table 5
The influence of the wake on the stability of the system with various values of μ

μ	Short plates		Long plates	
	0.2	0.6	4	20
U_{R_c}	9.92	6.71	10.15	8.71
$U^{\star}_{R_c}$	5.71	7.04	10.33	8.21
$\lvert U_{R_c} - U^{\star}_{R_c}\rvert$	4.21	0.35	0.18	0.50
$\lvert(U_{R_c}/\mu) - (U^{\star/\mu)}_{R_c}\rvert$	21.05	0.58	0.045	0.025

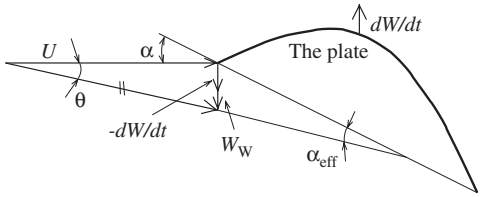

Fig. 8. A short plate and the flow conditions.

Table 6
The short plate studied by Kornecki et al. [6]

μ	U_{R_c}	$U_{R_c}^{\star\star}$	$\lvert U_{R_c} - U_{R_c}^{\star\star}\rvert$	$\lvert(U_{R_c}/\mu) - (U_{R_c}^{\star\star}/\mu)\rvert$
0.232	5.93	0.582	5.32	22.93

thus increase the effective angle of incidence α_{eff}. It follows that the lift, which would destabilize the plate, grows. Therefore, a smaller value of the critical flow velocity U_c can be expected, i.e., U_c would be underestimated. It should be emphasized that this simple theory can only be used for a very short plate ($\mu = 0.2$). With increasing values of μ, the vibration of the plate becomes more complex, and it is not adequate to represent the vibrating flexible plate with distributed $\mathrm{d}W(X)/\mathrm{d}t$ (which may not be in phase at different X) and $W_W(X)$ as a rigid airfoil with a single $\mathrm{d}W/\mathrm{d}t$ and a single W_W.

As a supplement to Table 5, a well-deserved mention is made of the work by Kornecki et al. [6] who studied a system with $\mu = 0.232$. In this work, a full model based on Theodorsen's theory was used for predicting the critical point (U_{R_c} as listed in Table 6), as well as a quasi-static model neglecting the motion of the plate for another critical point (denoted by $U_{R_c}^{\star\star}$ in Table 6). Note that neglecting the motion of the plate, instead of neglecting the wake (refer to Fig. 8 and the discussion in the foregoing) also significantly *changes* the value of the critical point for a short plate.

6. Concluding remarks

It is well known that a challenging difficulty in the problem of stability of a cantilevered flexible plate in axial flow arises from the finite length of the plate; a wake exists and affects the system dynamics. However, from a physical point of view, when the length of the plate is sufficiently large so as to approach an infinitely long plate, the influence of the wake on the system dynamics should diminish and then disappear (recall the much improved agreement for long plates shown in Fig. 3, between the theoretical predictions of Shelley et al. [18] and others [8,11,14,17] as well as the present theory). In this paper, we have studied the influence of the wake on the stability of cantilevered plates in axial flow and the underlying mechanisms.

In order to compare the flutter boundaries predicted/measured by various theories/experiments, the non-dimensional mass ratio μ and reduced flow velocity U_R are used as parameters. However, as the parameters μ and U_R share some physical elements, a monotonic trend cannot be observed in the U_{R_c} versus μ plot. To resolve this problem, all flutter boundaries are presented in a U_{R_c}/μ versus μ plot, in which a clear monotonic trend in the relation between the *dimensional* parameters U_c and L is discovered, supposing that the parameters ρ_P, h, D and ρ_F remain fixed. To this end, using U_{R_c}/μ as the ordinate in Fig. 3 does not just simply represent the theoretical/experimental data in a different way (refer to Fig. 9 in Ref. [14], which has been extensively used in other publications); it reveals an intrinsic property of the system, with direct physical meaning.

Taking advantage of the clear trend in the U_{R_c}/μ versus μ plot, a global assessment of the flutter boundaries by various theories and experiments can be made: the various theories (no matter whether they consider a wake or not) and experiments (where a wake always exists) agree with one another very well for long plates. However, for short plates, various theoretical predictions and experimental measurements exhibit quite large discrepancies. These observations immediately lead to the conclusion that the wake has less influence on

system stability for long plates than it does for short ones. As mentioned in the precursor paper [22], all influencing factors including the length of leading rigid segment, the level of material damping, the aspect ratio (for three-dimensional considerations) and so on, have less effect on system stability for long plates than they do for short ones. However, in the present paper, we have focussed on the influence of the wake and its effect on flutter.

It should be emphasized that the only conclusion that we have been able to reach with confidence is deliberately limited to the different levels of influence of the wake on stability, respectively for long and short plates; whether the existence of the wake *per se* would stabilize or destabilize the system is not discussed in the present paper. Moreover, although quantitative analysis has frequently been used, the assessment of the importance of the wake, regarding the level of its influence on system stability, is still qualitative.

To evaluate the influence of a dynamic wake is not an easy task. First, an accurate model of the wake and the unsteady flow conditions surrounding an oscillating deformable solid body requires sophisticated and refined knowledge, to a level not yet attainable—to the authors' knowledge. Second, influences of various parameters in such a complex system as a cantilevered plate in axial flow are normally interwoven, and they do not necessarily have a monotonic/uniform pattern in terms of a specific parameter; this fact would make an assessment of the influence of the wake even more complicated. However, the observed overall trend of the flutter boundary in Fig. 3 is so starkly clear that a relatively simple wake model and the associated analytical approach used in the current paper can and do reveal the underlying mechanism of the influence of the wake, with a fairly high degree of confidence.

Through a carefully arranged study on the dynamics of the system along the flutter boundary, it is found that longer plates have higher critical frequencies, which lead to shorter wavelengths in the wake and consequently to smaller wake-induced flow velocities (*downwash*) on the plate. On the other hand, more higher-order mode components are found in the plate vibration at the critical point for longer plates, which, in conjunction with the higher critical frequencies, result in higher overall plate vibration velocities. Under the combined action of these two factors, the ratio of plate vibration velocity to wake-induced flow velocity becomes higher for longer plates; therefore, it can be concluded that for longer plates the wake has a smaller influence.

Acknowledgements

The authors gratefully acknowledge the support by the Natural Sciences and Engineering Research Council of Canada (NSERC) and Le Fonds Québécois de la Recherche sur la Nature et les Technologies (FQRNT) of Québec; the leading author also gratefully acknowledges the support by a NSERC scholarship and a McGill Graduate Studies Fellowship.

References

[1] S. Taneda, Waving motions of flags, *Journal of the Physical Society of Japan* 24 (1968) 392–401.
[2] S.K. Datta, W.G. Gottenberg, Instability of an elastic strip hanging in an airstream, *Journal of Applied Mechanics* 42 (1975) 195–198.
[3] J. Zhang, S. Childress, A. Libchaber, M. Shelley, Flexible filaments in a flowing soap film as a model for one-dimensional flags in a two-dimensional wind, *Nature* 408 (2000) 835–839.
[4] Y. Yadykin, V. Tenetov, D. Levin, The flow-induced vibration of a flexible strip hanging vertically in a parallel flow, part 1: temporal aeroelastic instability, *Journal of Fluids and Structures* 15 (2001) 1167–1185.
[5] C. Lemaitre, P. Hémon, E. de Langre, Instability of a long ribbon hanging in axial air flow, *Journal of Fluids and Structures* 20 (2005) 913–925.
[6] A. Kornecki, E.H. Dowell, J. O'Brien, On the aeroelastic instability of two-dimensional panels in uniform incompressible flow, *Journal of Sound and Vibration* 47 (1976) 163–178.
[7] L.K. Shayo, The stability of cantilever panels in uniform incompressible flow, *Journal of Sound and Vibration* 68 (1980) 341–350.
[8] L.X. Huang, Flutter of cantilevered plates in axial flow, *Journal of Fluids and Structures* 9 (1995) 127–147.
[9] T. Balint, A.D. Lucey, Instability of a cantilevered flexible plate in viscous channel flow, *Journal of Fluids and Structures* 20 (7) (2005) 893–912.
[10] C.Q. Guo, M.P. Païdoussis, Stability of rectangular plates with free side-edges in two-dimensional inviscid flow, *Journal of Applied Mechanics* 67 (2000) 171–176.

[11] N. Yamaguchi, K. Yokota, Y. Tsujimoto, Flutter limits and behaviors of a flexible thin sheet in high-speed flow–I: analytical method for prediction of the sheet behavior, *ASME Journal of Fluids Engineering* 122 (2000) 65–73.
[12] N. Yamaguchi, T. Sekiguchi, K. Yokota, Y. Tsujimoto, Flutter limits and behaviors of a flexible thin sheet in high-speed flow—II: experimental results and predicted behaviors for low mass ratios, *ASME Journal of Fluids Engineering* 122 (2000) 74–83.
[13] Y. Watanabe, S. Suzuki, M. Sugihara, Y. Sueoka, An experimental study of paper flutter, *Journal of Fluids and Structures* 16 (2002) 529–542.
[14] Y. Watanabe, K. Isogai, S. Suzuki, M. Sugihara, A theoretical study of paper flutter, *Journal of Fluids and Structures* 16 (2002) 543–560.
[15] D.M. Tang, H. Yamamoto, E.H. Dowell, Flutter and limit cycle oscillations of two-dimensional panels in three-dimensional axial flow, *Journal of Fluids and Structures* 17 (2003) 225–242.
[16] P.J. Attar, E.H. Dowell, D.M. Tang, Modeling aerodynamic nonlinearity for two aeroelastic configurations: delta wing and flapping flag, *Proceedings of the 44th AIAA/ASME/ASCE/AHS Structures, Structural Dynamics, and Materials Conference*, 2003, pp. 12–22.
[17] M. Argentina, L. Mahadevan, Fluid-flow-induced flutter of a flag, *Proceedings of the National Academy of Science of the United States of America* 102 (2005) 1829–1834.
[18] M. Shelley, N. Vandenberghe, J. Zhang, Heavy flags undergo spontaneous oscillations in flowing water, *Physical Review Letters* (094302) (2005) 1–4.
[19] C. Souilliez, C. Eloy, L. Schouveiler, An experimental study of flag flutter, *Proceedings of PVP2006-ICPVT-11*, 93864.
[20] C. Eloy, C. Souilliez, L. Schouveiler, Flutter of a rectangular cantilevered plate, *Proceedings of PVP2006-ICPVT-11*, 93837
[21] M.P. Païdoussis, *Fluid–structure Interactions. Slender Structures and Axial Flow*, Vol. 2, Elsevier Academic Press, London, 2004.
[22] L. Tang, M.P. Païdoussis, On the instability and the post-critical behaviour of two-dimensional cantilevered flexible plates in axial flow, *Journal of Sound and Vibration* 305 (2007) 97–115.
[23] J. Katz, A. Plotkin, *Low-Speed Aerodynamics*, second ed., Cambridge University Press, New York, 2001.
[24] C. Semler, G.X. Li, M.P. Païdoussis, The non-linear equations of motion of pipes conveying fluid, *Journal of Sound and Vibration* 165 (1992) 577–599.
[25] J.C. Snowdon, *Vibration and Shock in Damped Mechanical Systems*, first ed., Wiley, New York, 1968.
[26] J.D. Anderson, *Fundamentals of Aerodynamics*, third ed., McGraw-Hill, Boston, 2001.
[27] R.E.D. Bishop, D.C. Johnson, *The Mechanics of Vibration*, Cambridge University Press, Cambridge, 1979.
[28] R.L. Bisplinghoff, H. Ashley, R.L. Halfman, *Aeroelasticity*, first ed., Addison-Wesley, Reading, MA, 1955.
[29] D.G. Crighton, J.E. Oswell, Fluid loading with mean flow. I. Response of an elastic plate to localized excitation, *Philosophical Transactions of Royal Society of London* 335 (1991) 557–592.